Hemodialysis vascular access failure: novel pathophysiological mechanisms and therapeutic strategies

Bezhaeva, T.

Chapter 4

Relaxin receptor deficiency promotes vascular inflammation and impairs outward remodeling in arteriovenous fistulas

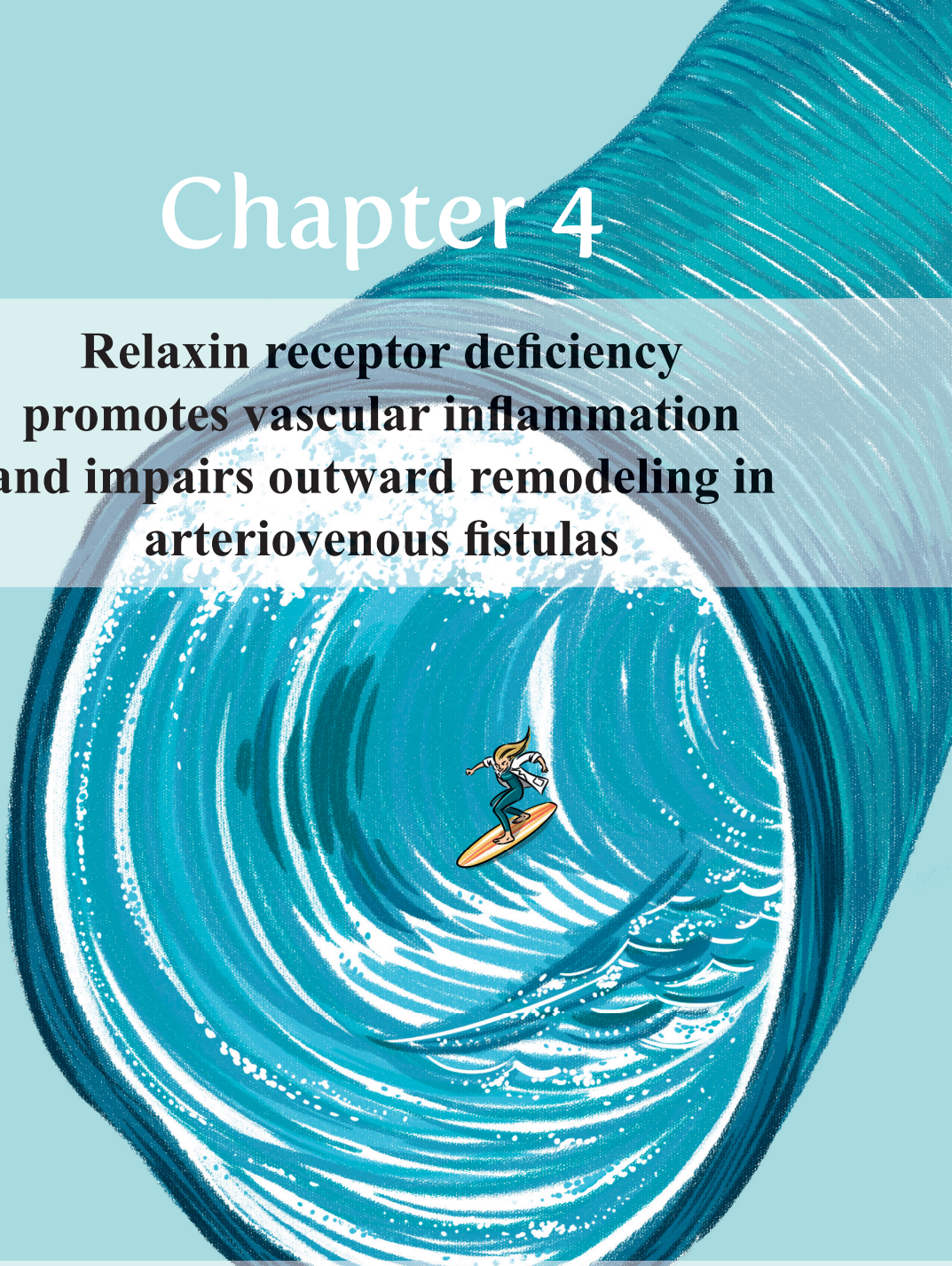

Taisiya Bezhaeva, Margreet R. de Vries, Wouter J. Geelhoed, Eric P. van der Veer, Sabine Versteeg Carla M.A. van Alem, Bram M. Voorzaat, Niels Eijkelkamp, Koen E. van der Bogt, Alexander I. Agoulnik, Anton Jan van Zonneveld, Paul H.A.Quax and Joris I. Rotmans

FASEB. 2018 Nov Vol.32

Abstract

The pathophysiology of arteriovenous fistula (AVF) maturation failure is incompletely understood but impaired outward remodeling and intimal hyperplasia are considered to contribute. This adverse vascular response upon AVF surgery results from an interplay between vascular smooth muscle cells (VSMCs), extracellular matrix (ECM) and inflammatory cells. Relaxin (RLN) is a hormone exhibiting its action on the vasculature via interaction with its receptor (RXFP1), resulting in vasodilatation, ECM remodeling and decreased inflammation. In the present study, we evaluated the consequences of RXFP1 knockout (*Rxfp1*$^{-/-}$) on AVF maturation in a murine model of AVF failure. At 14 days after AVF surgery, *Rxfp1*$^{-/-}$ mice showed a 22% decrease in vessel size at the venous outflow tract. Furthermore, a 43% increase in elastin content was observed in the lesions of *Rxfp1*$^{-/-}$ mice which coincided with a 41% reduction in elastase activity. In addition, *Rxfp1*$^{-/-}$ mice displayed a 6-fold increase in CD45^{+} leukocytes, along with a 2-fold increase in MCP1 levels, when compared to WT mice. *In vitro*, VSMCs from *Rxfp1*$^{-/-}$ mice exhibited a synthetic phenotype, as illustrated by augmentation of collagen, fibronectin, TGFβ and PDGF mRNA. In addition, VSMCs derived from *Rxfp1*$^{-/-}$ mice showed a 5-fold increase in cell migration. Finally, RXFP1 and RLN expression levels were increased in human AVFs, as compared to unoperated cephalic veins. In conclusion, RXFP1 deficiency hampers elastin degradation and results in induced vascular inflammation after AVF surgery. These processes impair outward remodeling in murine AVF, suggesting that the relaxin-axis could be a potential therapeutic target to promote AVF maturation.

Introduction

A proper functioning vascular access site is a lifeline for a lifetime for patients required hemodialysis. While an arteriovenous fistula (AVF) remains the vascular access of choice, the frequency of primary AVF failure is approximately 40%[1]. Moreover, the primary patency rates at 1 year after creation do not exceed 60%[2], making vascular access related complications one of the most common causes of hospitalization and morbidity in hemodialysis patients.

While the pathophysiology of arteriovenous fistula maturation failure is incompletely understood, it is well established that both intimal hyperplasia (IH) and outward remodeling (OR) of the arteriovenous conduit ultimately determine luminal dimensions, fistula flow and patency[3]. Several studies have shown that vascular adaptation of the arteriovenous conduit is characterized by an inflammatory response that coincides with flow-mediated remodeling of the extracellular matrix (ECM) and proliferation and migration of vascular smooth muscle cells (VSMCs)[4-11].

Relaxin (RLN) is a 6-kDa peptide hormone, originally known for its role in the growth and differentiation of the reproductive tract, and systemic hemodynamic adaptations during pregnancy, in particular vasodilatation[12-15]. Three relaxin genes, namely relaxin-1, -2, and -3 (*RLN1*, *2* and *3*) exist in humans, whereas rats and mice have two (*Rln1* and *3*), with *Rln1* in rats and mice corresponding to human RLN2 and representing the major source of circulating relaxin[16]. In the last 20 years, relaxin has emerged as a pleotropic hormone that serves critical functions irrespective of gender. The systemic effects mediated by RLN2 on arterial mechanical properties include increasing arterial compliance, reducing systemic vascular resistance, and myogenic reactivity as demonstrated in rats and mice[12,17-20].
Furthermore, administration of recombinant RLN2 ameliorates renal and cardiac fibrosis, stimulates ECM turnover, and moderates inflammation by reducing inflammatory cytokines[21-27].

In the context of AVF maturation, it is important to emphasize that RLN2 is expressed in the vessel wall[28,29] and that the observed vascular effects of RLN2 are mediated though an interaction with RXFP1 (relaxin/insulin-like peptide family receptor 1, original abbreviation LGR7), a G-protein-coupled receptor. RXFP1 is primarily expressed on VSMCs and to a lesser extent on the cell surface of macrophages and endothelial cells of arteries and veins[30-32].

In view of the emerging role of the RLN2-RXFP1 axis in vascular remodeling and inflammation, we examined the consequences of disturbing this hormone-receptor balance in AVF maturation. For this purpose, we used the well-established murine AVF model in which we studied the effect of RXFP1 deficiency on fistula remodeling. Furthermore, we determined the effects of RXFP1 deficiency on the phenotype and function of VSMCs *in vitro.*

Material and Methods

Animals

Murine model of AVF failure

This study was performed in agreement with Dutch government guidelines and the Directive 2010/63/EU of the European Parliament. All animal experiments were approved by the Institutional Committee for Animal Welfare of Leiden University Medical Center and University Medical Center Utrecht. The phenotype of *Rxfp1*$^{-/-}$ mice was described previously[33]. Male wild type (WT, C57BL/6, n=10) and *Rxfp1*$^{-/-}$ mice (C57BL/6 background, n=10), were bred in the animal facility at the University Medical Center Utrecht. All animals were given water and chow ad libitum. Adult male mice aged 10-13 weeks were used for the experiments. AVF were created in an end-to-side manner between the dorsomedial branch of the external jugular vein and the common carotid artery as previously described[5,34]. In short, the animal was anesthetized using isoflurane followed by shaving and disinfection of the skin in the ventral neck area and fixed in a supine position on a heating blanket. The mouse was then injected with buprenorphin (0.1 mg/kg) (MSD, USA) and 0.5 mL saline. Under a dissecting microscope (Leica, Germany), an incision in the ventral midline of the neck area was made, followed by a dissection of the right dorsomedial branch of the external jugular vein and ipsilateral common carotid artery after the excision of the sternocleidomastoid muscle using a heat cauterizer. Next, after applying a vascular clamp (S&T, Switzerland) on the proximal and distal artery an approximate 1 mm incision was made using a microscissor (Fine Science Tools, Germany) and the lumen was rinsed with a heparin solution (100 IU/ml) (LEO Pharma, Denmark). The vein was then clamped proximally and ligated distally, followed by a transection just proximal to the ligation. After rinsing the vein with a heparin solution, an end-to-side anastomosis was created using 10.0 interrupted sutures (BBraun, Germany). After completion of the anastomosis, the remaining clamps were removed and patency was assessed. The skin was closed with a 6.0 running suture (BBraun, Germany). Following completion of the surgery 0.5 mL of saline was injected subcutaneously and the mice were kept warm until recovery. The animals were sacrificed 14 days following the surgical procedure.

Blood pressure

Systolic blood pressure was assessed with the non-invasive tail cuff system in conscious mice before the AVF surgery and at day 7 and 14 after an AVF was created using the CODA system (Kent Scientific, CT, USA). Animals were acclimated to the restrainer before measurements. Following the acclimation period, telemetry blood pressure measurements were acquired. Ten seconds data segments were collected throughout the duration of each noninvasive measurement session (10 acclimation cycles followed by 20 measurement cycles).

Arterial compliance

Aortas from *Rxfp1*$^{-/-}$ (n=3) and WT (n=5) mice were cannulated from the distal side at the base of the heart and proximal at the abdominal area (1 cm of length) and placed immediately in ice-cold HEPES buffered physiological saline solution. Consequently, the vessels were placed in an *ex vivo* vessel perfusion system containing 37^0C 10^{-4} M

papaverine in calcium-free HEPES buffered physiologic saline solution. The vessel segments were tensioned to a longitudinal strain of 30 g and left to acclimatize for 15 minutes. The vessel segment was then exposed to a pressurized flow in a cyclic fashion at 60 BPM ± 5 BPM, where the systolic pressure was gradually increased to 120 mmHg. Papavarin (10^{-4}M) in calcium-free HEPES buffered PBS was used as perfusate. The systolic and diastolic pressures throughout the test were recorded using a pressure sensor (700 G Precision Pressure Test Gauge, Fluke, Singapore). To measure the vessel diameter a microscope camera (Digital microscope DSCO-P03, Frederiksen Scientific, Denmark) capable of measuring with an accuracy of ± 0.02 mm was placed above the perfused vessels. Recordings of each test was calibrated to the pressure and saved. To calculate arterial compliance, the vessel diameter during the systolic and diastolic phase of the pressure cycles, were measured. The dynamic compliance is provided as % compliance per 100 mmHg.

Tissue harvesting and processing

Fourteen days after AVF surgery, the animals were anesthetized using isoflurane. The venous and arterial limb of the AVF was dissected and a thoracotomy was performed whereupon the inferior vena cava was transsected followed by a fixation with 4% formalin through an intracardiac perfusion. The tissue was embedded in paraffin and 5 µm-thick sections of the venous outflow tract were made perpendicular to the vein at 150 µm interval.

Morphometric and histological analysis

All (immuno)-histochemical stainings and measurements were performed on the first 3 venous cross-sections downstream from the area of anastomosis. Weigert's elastin staining was used for the morphometric measurements. The area of the internal elastic lamina (IEL) was measured to assess the degree of the outward remodeling (Figure 1a). Intimal hyperplasia was calculated by subtracting the luminal area from the area within the IEL. Composition of the AVF lesions was further evaluated by staining for total leukocytes (CD45, 1:200; BD- Pharmingen 550539, CA, USA), macrophages (MAC3, 1:200, BD-Pharmingen 550292, CA, USA) in a combination with CCR2 for pro-inflammatory phenotype (1:400, Abcam ab32144, Cambridge, UK) or CD206 (1:1000, Abcam ab64693, Cambridge, UK) for anti-inflammatory phenotype, neutrophils (GR1, 1:300, from G. Kraal, VUMC, The Netherlands), T-lymphocytes (CD3, 1:300, Abcam ab32144, Cambridge, UK) and MCP1 (MCP1, 1:300, Santa Cruz sc-1784, Texas, USA) vascular smooth muscle cells (SM-α-actin, 1:1000, Dako M0851, CA, USA) was stained in a combination with Ki67 (1:200, BD-Pharmigen 550609, CA, USA) to detect proliferating VSMCs.

All slides were digitized using an automated microscopic scanner (Pannoramic digital MIDI, 3DHISTECH, Budapest, Hungary). For the immunohistochemical analysis of the MAC3/CD206, MAC3/CCR2 and αSMA/Ki67 staining, the number of positive cells was counted in 3 random fields of view using a 400x magnification from which the mean was calculated. Quantification of $CD45^+$, $GR1^+$, $CD3^+$ and MCP1 staining was performed with ImageJ software by calculating % DAB positive area from the total vessel area.

Cell culture

Vascular smooth muscle cells

Primary arterial and venous vascular smooth muscle cells were isolated from murine carotid artery and vena cava of C57BL/6 and *Rxfp1*$^{-/-}$ mice (n=4 per group), respectively. Connective tissues were removed and vessels cut open. The endothelial monolayer was detached by gentle scraping using sterile surgical forceps. The carotid artery and caval vein were dissected into small pieces and plated onto fibronectin pre-coated petri dishes (0.1 mg/mL) of 100 or 60 mm diameter. After 14 days of culture with DMEM medium supplemented with 20% fetal calf serum (FCS), 2 mM L-glutamine, 100 U/ml penicillin and 100 μg/ml streptomycin, cells were trypsinized and re-plated onto 6- or 12-well plates and cultured for 7 days. At 80-90% confluence, VSMCs were trypsinized and seeded at required density for further functional assays.

Western Blotting

Proteins from tissue lysates were harvested in RIPA buffer and subjected to polyacrylamide gel electrophoresis. Protein determinations (BCA) were performed to ensure equal loading of protein on a per-sample basis. RXFP1 was detected using primary antibodies (1:500, Acris AP23446SU-S, MD, USA). GAPDH (1:5000, Cell signaling 5174S, MA, USA) was used as a loading control. All gels were run and blotted with Bio-Rad TGX pre-cast gels and blotted on nitrocellulose 0.2 μm using the Bio-Rad TurboBlot system (Bio-Rad Laboratories, CA, USA).

RNA isolation, cDNA synthesis and qPCR

Total RNA was extracted from VSMCs using Trizol reagent (Invitrogen, CA, USA) according to the manufacturer's protocol. RNA was reverse transcribed by M-MLV First-Strand Synthesis system (Invitrogen, CA, USA), and used for quantitative analysis of mouse genes (Supplementary Table 1) with an SYBR Green Master Mix (Applied Biosystems, CA, USA). Murine β-actin was used as standard housekeeping gene. The relative mRNA expression levels were determined using 2[–ΔΔC(T)] method.

VSMC migration and haptotaxis assays

Primary arterial and venous VSMCs from control and *Rxfp1*$^{-/-}$ mice were grown to confluence and made quiescent in cultured medium supplemented with 1% FCS for 24 hours. Cells were detached from the surface and suspended at a concentration of 100.000 cells/mL in culture medium supplemented with 1% FCS. Migration was assayed with inserts having 8 μm-pores in 24-well chemotaxis chambers using commercial CytoSelect Cell Migration Assay Kit. Haptotaxis was assayed by plating cells into Transwell inserts with collagen I-coated inserts (CytoSelect Cell Haptotaxis Assay, Cell Biolabs, CA, USA). After 16 hours, migratory VSMCs were lysed and labeled with fluorescent dye according to the manufacturer's instructions. 20% FCS was used as gradient. Quantification was performed by reading fluorescence at 480 nm/520 nm.

VSMC proliferation assay

Murine VSMCs, explanted from aortas and veins of control or *Rxfp1*$^{-/-}$ mice, were cultured as described above and aliquoted into a 96-well plate. All cell numbers were subsequently determined 24 hours later using the CyQuant Direct Cell Proliferation

Assay as per the manufacturer's instructions (Life Technologies, CA, USA).

Elastase activity assay
Elastase activity was measured on total tissue lysates isolated from *Rxfp1*$^{-/-}$ and WT mice (n=10 per group) using the EnzChek Assay Kit (Thermo Fisher Scientific, MA, USA) according to the manufacturer's instructions. Briefly, 10 μm sections of AVF were lysed in RIPA buffer and protein determinations (BCA) was performed to ensure equal loading of protein on a per-sample basis. DQ™ elastin , a soluble bovine neck ligament elastin labeled with BODIPY® FL dye, was used as a substrate such that the conjugate's fluorescence is quenched. In the presence of elastase, the non-fluorescent substrate is digested yielding highly fluorescent fragments which is measured with a microplate reader at ex/em = 480 ± 20 nm/528 ± 20 nm.

Collagen assay
Collagen was analyzed in formaldehyde-fixed paraffin-embedded venous tissues isolated from *Rxfp1*$^{-/-}$ and WT mice (n=10 per group) using QuickZyme Total Collagen Assay Kit (QuickZyme Biosciences, the Netherlands). In brief, five to ten 10 μm tissue sections were hydrolyzed by o/n incubation at 95°C in a heat block. Upon hydrolysis, without any pretreatment, 35 μl was used for collagen quantification using the QuickZyme total collagen assay (assay time 90 min). The assay measured the total amount of hydroxyproline present in the sample, which represents all collagen-types present in the sample. The assay results in a chromogen with an absorbance maximum at 570 nm.

Human tissue specimens
Human cephalic veins before AVF surgery (n=3) and during surgical revisions of AVF (n=3) were obtained at the Leiden University Medical Center in accordance with guidelines set out by the 'Code for Proper Secondary Use of Human Tissue' of the Dutch Federation of Biomedical Scientific Societies (Federa) and conform with the principles outlined in the Declaration of Helsinki. Specimens were formalin fixed, embedded in paraffin and sectioned. The human AVF sections were stained with SM-α-actin (1:1000, DAKO M0851, CA, USA), RLX2 (RLN2, 1:1000, Abcam ab183505, Cambridge, UK) and RXFP1 (1:4000, Acris AP23446SU-S, MD, USA).

For RXFP1 antibody validation 3 human fistula samples were incubated with the primary antibody or isotype control both at 1:4000 dilution. Human endometrium was used as a positive control. Briefly, after deparaffinization step endogenous peroxidase was suppressed by incubation in 1% H_2O_2 for 15 min at room temperature (RT). Sections were then blocked with 5% PBSA ($NaPO_4$, NaCl, NaAz and 1% bovine serum albumin) and 5% NHS (normal human serum) for 30min. Next, sections were incubated with the primary antibody or isotype control, diluted at 1:4000 in 1% PBSA buffer together with 5% NHS, overnight at RT. After rinsing 3 × 5 min in PBS, sections were then incubated with rabbit Evision (Agilent Dako, CA, USA) and 5% NHS for 30min at RT. Specific signals were detected using DAB (Sigma-Aldrich, MO, USA) as chromogen, stopping the reaction by rapidly rinsing in tap water, followed by conventional haemalaun counterstaining.

For immunofluorescent staining of double positive αSMA^{+}, RXFP1^{+} cells, after primary antibody sections were counterstained with Alexa 568 conjugated goat anti mouse IgG2a (1:250; Molecular probes A21134, MA, USA), for SM-α-actin and Alexa 488 conjugated secondary goat anti rabbit IgG (1:250; Molecular probes A11008, MA, USA) for RXFP1. Secondary antibody were diluted in 1% PBSA and 5% NHS was added to prevent nonspecific binding. Nuclei were visualized with ProLong™ Gold Antifade Mountant with DAPI (Thermo Fisher P369, MA, USA) (Supplemental Figure 6).

Statistical analysis

Results are expressed as mean±SEM and considered statistically significant for $P<0.05$. T-tests and Mann-Whitney tests for parametric and nonparametric data, respectively, were used as appropriate. All *in vitro* experiments were performed in biological n=4 in experimental triplicates.

Results

Surgical outcome and patency

In total, 23 mice were successfully operated and received an AVF (WT; n=12, *Rxfp1*$^{-/-}$; n=11), of which two (17%) from the wild-type (WT) group and one (9%) from the *Rxfp1*$^{-/-}$group were occluded 14 days after surgery. The occluded AVFs were excluded from morphometric analysis, yielding 10 animals per group. The body weight of the mice was similar in both groups (29±3 gram) and remained stable until the end of experiment.

Effect of RXFP1 deficiency on AVF maturation

To study the effect of RXFP1 deficiency on AVF maturation, we created AVFs in WT and *Rxfp1*$^{-/-}$ mice in an end-to-side fashion between the jugular vein and carotid artery as described previously[34]. Given that most of the stenotic lesions in human AVF occur in the venous outflow tract, we harvested the first three consecutive venous sections downstream of the anastomotic area for morphometric analysis. The impact of RXFP1 deficiency on vessel morphometry was evaluated by assessing both intimal and luminal area as well as the area within the internal elastic lamina (IEL), reflecting the degree of outward remodeling of the venous outflow tract (Figure 1a). The absence of the RXFP1 protein in *Rxfp1*$^{-/-}$ mice was confirmed by analyzing total tissue lysates isolated from jugular veins by Western blotting (Figure 1b). Mice deficient for RXFP1 showed a 22% decrease of the IEL area at the venous outflow tract when compared to WT mice ($P=0.002$). The luminal area of the venous outflow tract in *Rxfp1*$^{-/-}$ mice was 31% smaller when compared to control mice, although this difference was not significant ($P=0.14$). The intimal area did not differ between groups (Figure 1c). Arterial blood pressure and compliance did not significantly differ between *Rxfp1*$^{-/-}$ and WT mice (Supplemental Figure 1).

In terms of ECM remodeling, we observed a 43% increase in elastin content in *Rxfp1*$^{-/-}$ mice as compared to WT mice ($P=0.04$) (Figure 1d), while collagen production was similar between the groups (Supplemental Figure 2). In both WT and *Rxfp1*$^{-/-}$ mice, the majority of intimal cells expressed SM-α-actin, indicating that these cells are primarily of VSMC or fibroblastic origin (Figure 1e).

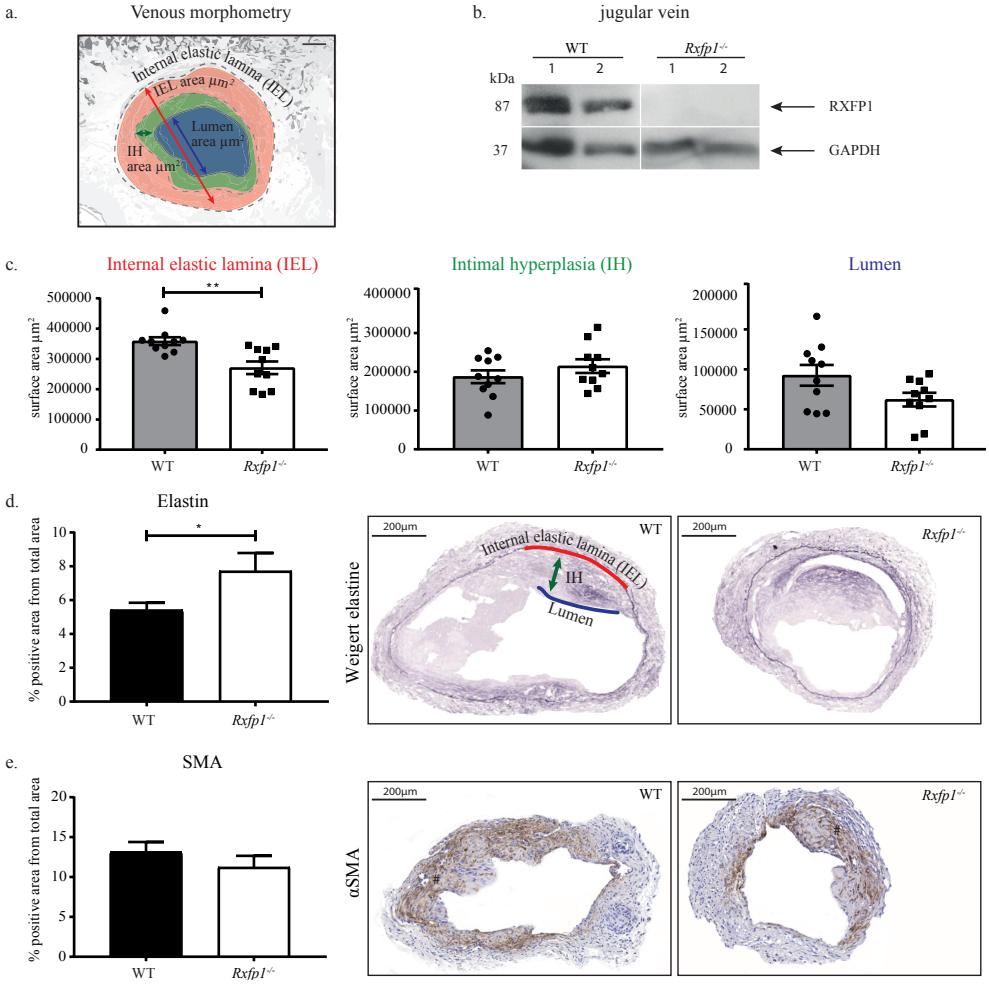

Figure 1. Morphometry and histology of the venous outflow tract of the AVF in *Rxfp1*$^{-/-}$ and WT mice 14 days after surgery.

(a) The area within the internal elastic lamina (IEL) (red), reflects the degree of outward remodeling of the venous outflow tract. Intimal hyperplasia (green) was calculated by subtracting the luminal area (blue) from the area within the IEL. (b) Western blotting of the jugular vein confirms the absence of RXFP1 protein in RXFP1 deficient mice, GAPDH was used as a loading control. (c) Quantification of histomorphometry. RXFP1 deficient mice displayed decrease in the area of IEL (22%, P=0.002) and lumen (31%, P=0.14), whereas intimal hyperplasia was comparable to WT mice. (d) Increase in elastin deposition in the AVF lesions from *Rxfp1*$^{-/-}$ mice. (e) SM-α-actin (αSMA) staining shows area of intimal hyperplasia which did not differ between the groups. Weigert elastine staining was used to determine histomorphometrical parameters of the vessel. (#) intimal hyperplasia; (*) P<0.05; (**)P<0.005 n=10 per group.

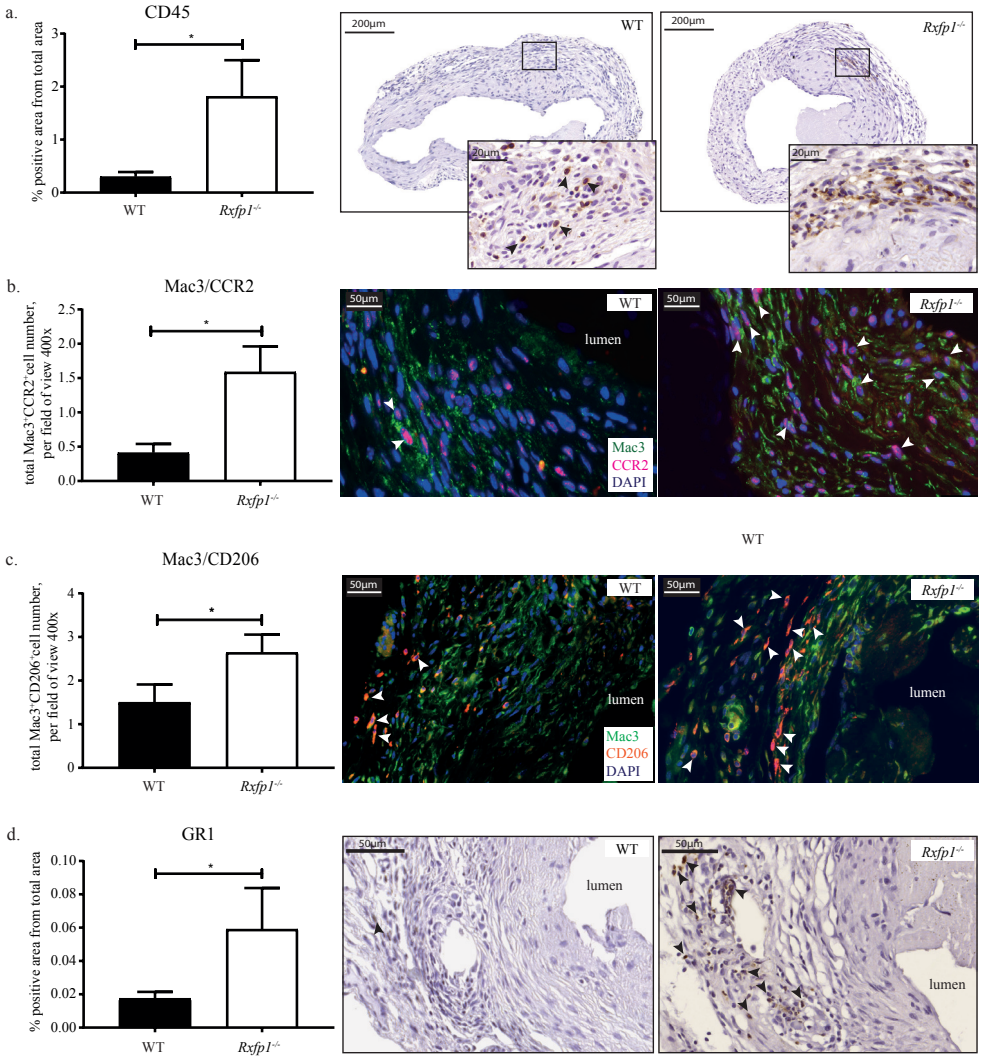

Figure 2. Effects of RXFP1 deficiency on inflammatory status *in vivo*.
Quantification and immunohistochemical staining of (a) CD45⁺ leukocytes (black arrows); (b) MAC3⁺/CCR2⁺ macrophages, (c) MAC3⁺/CD206⁺ macrophages (white arrows), and (d) GR1⁺ neutrophils (black arrows) in the AVF lesions 14 days after surgery. All cell populations were increased in the lesions from *Rxfp1*$^{-/-}$ mice as compared to WT. (*) P<0.05; n=10 per group.

RXFP1 deficiency resulted in increased inflammation of AVF lesions

Immunohistochemical analysis of sections obtained from the venous outflow tract showed a 6-fold increase in the amount of CD45⁺ leukocytes in lesions of *Rxfp1*$^{-/-}$ mice as compared to WT mice (P=0.02) (Figure 2a). As shown in Figure 2b-c, further characterization of the leukocyte subpopulations revealed a 4-fold increase in the number of pro-inflammatory Mac3⁺/CCR2⁺ macrophages (P=0.02) and a 43% increase

in the Mac3^{+}/CD206^{+} anti-inflammatory macrophages in the lesions from *Rxfp1*$^{-/-}$ mice (P=0.04). The number of GR1^{+} neutrophils was 3-fold higher in *Rxfp1*$^{-/-}$ mice as compared to WT mice (P=0.05) (Figure 2d). The number of CD3^{+} T-lymphocytes in the venous outflow tract was not affected by RXFP1 deficiency (Supplemental Figure 3). At the level of cytokine production within the lesions, a 2-fold increase of MCP1 expression was observed in *Rxfp1*$^{-/-}$ mice as compared to WT mice (P=0.01) (Figure 3). *In vitro*, activated macrophages differentiated from monocytes derived from *Rxfp1*$^{-/-}$ mice produced similar amounts of cytokines as compared to WT mice, as ELISA analysis demonstrated comparable expression of MCP1, IL12 and IL10 proteins (data not shown).

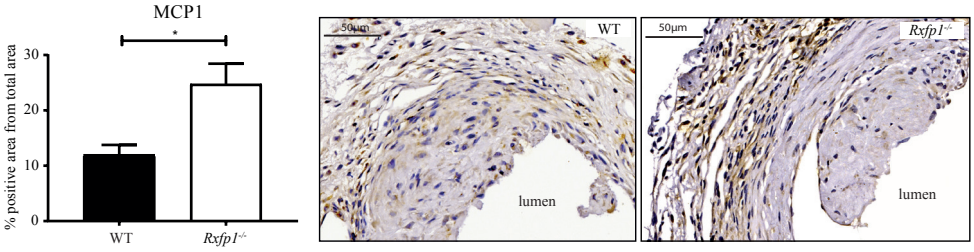

Figure 3. Accumulation of MCP1 in the AVF lesions from *Rxfp1*$^{-/-}$ and WT mice 14 days after surgery.
RXFP1 deficiency resulted in increased MCP1 expression (brown DAB signal) as compared to WT mice. (*) P<0.05; n=10 per group.

Phenotypic switch of arterial and venous VSMCs upon RXFP1 deletion

The impact of RXFP1 deficiency on VSMCs phenotype was studied *in vitro* using primary arterial and venous VSMCs, isolated from the aorta and caval vein of *Rxfp1*$^{-/-}$ or WT mice. Phenotypic difference of arterial and venous VSMCs was confirmed by mRNA levels of ephrin B2, an established embryological marker of arterial origin[35]. EphrinB2 was increased in arterial VSMCs from both WT and *Rxfp1*$^{-/-}$ mice following two weeks of culture as compared to venous VSMCs (Figure 4a). Further characterization of these VSMCs confirmed that the cells maintained a highly differentiated state, as evidenced by the maintenance of myosin heavy chain (MHC), calponin and caldesmon expression at two weeks of culture (Figure 4b).

As vascular injury and remodeling trigger the phenotypic switch of VSMCs from a contractile toward a synthetic state, mRNA expression levels of several genes associated with this switch were measured[36,37]. Arterial VSMCs from *Rxfp1*$^{-/-}$ mice expressed markedly higher levels of the synthetic VSMC markers type I collagen[38] and fibronectin[39] as compared to VSMCs derived from WT mice (5-fold, P=0.03; 10-fold, P=0.04; respectively). Similarly, type I collagen and fibronectin mRNA expression was augmented in venous VSMCs harvested from *Rxfp1*$^{-/-}$ mice (3-fold; P=0.05, and 4-fold; P=0.04, respectively). Furthermore, genes linked with cellular proliferation, such as transforming growth factor beta (TGFβ1)[40] and platelet derived growth factor (PDGF)[41], displayed on average 3-fold higher expression levels in both arterial and venous VSMCs isolated from *Rxfp1*$^{-/-}$ mice as compared to WT mice (Figure 4c).

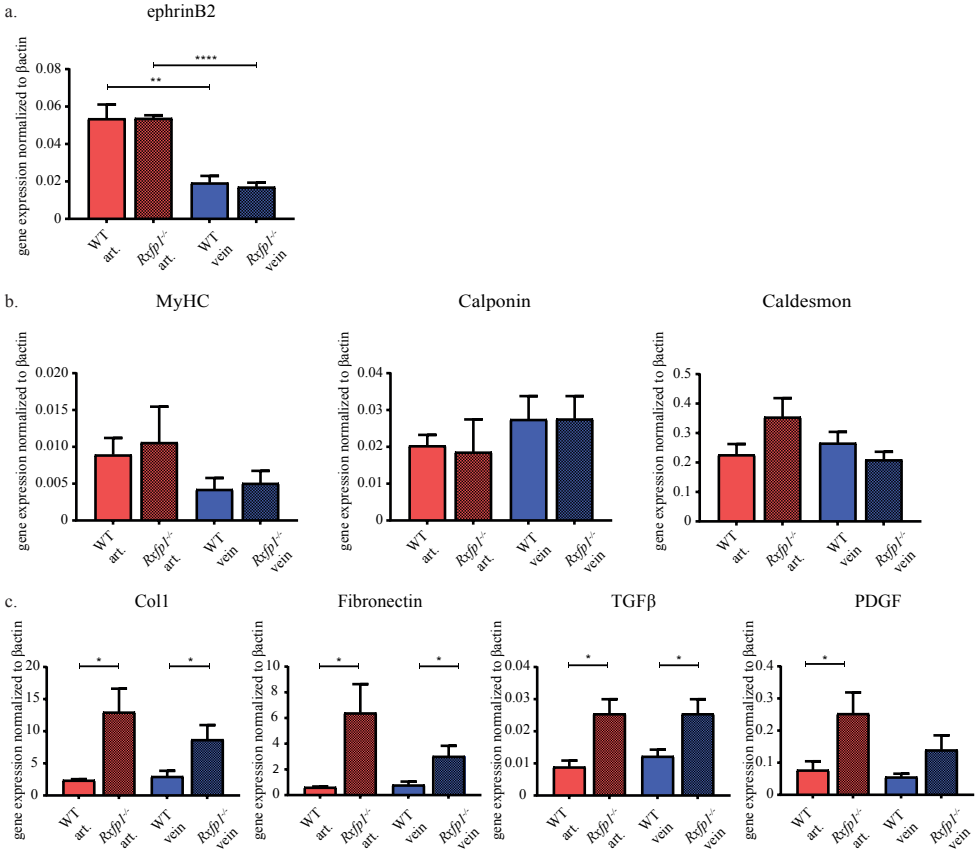

Figure 4. ***In vitro*** **phenotypic difference between primary arterial and venous VSMCs isolated from** ***Rxfp1*** $^{-/-}$ **and WT mice.**

(a) Stable increase in ephrinB2 gene expression was detected in arterial VSMCs isolated from WT and *Rxfp1* $^{-/-}$ mice. (b) Both arterial and venous VSMCs isolated from *Rxfp1* $^{-/-}$ and WT displayed characteristics of mature VSMCs as confirmed by a stable expression of myosin heavy chain (MYHC), calponin and caldesmon genes. (c) RXFP1 deficiency resulted in a switch of arterial and venous VSMCs towards synthetic phenotype as confirmed by increased collagen I (Col1), fibronectine, TGFβ and PDGF mRNA expression levels. VSMCs were maintained in culture for14 days. (*) P<0.05; (**) P<0.005; (****) P<0.0001; n=4.

To further examine whether relaxin deficiency impacts VSMC function, we performed cellular migration assays. These studies revealed that arterial VSMCs derived from *Rxfp1* $^{-/-}$ display a significantly higher migratory capacity relative to VSMCs derived from WT mice, while migration of venous VSMCs was unaltered (Figure 5a). To mimic VSMC migration within the ECM of a blood vessel, a haptotaxis assay was performed in which cellular migration was evaluated in a matrix of type I collagen. As shown in Figure 5b, we observed enhanced migration of arterial and venous VSMCs derived from *Rxfp1* $^{-/-}$ mice as compared to WT (5-fold, P=0.05; 5-fold; P=0.03; respectively). In contrast, cellular proliferation was not affected by relaxin deficiency in either arterial or venous VSMCs (Figure 5c). *In vivo*, the number of proliferating cells in the venous outflow tract of AVF did not differ significantly between groups (Supplemental Figure 4).

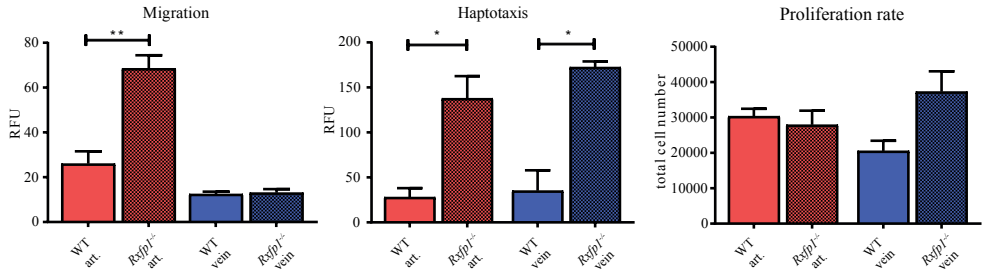

Figure 5. Effect of RXFP1 deficiency on VSMCs function *in vitro*.
(a) Increase in migration of VSMCs isolated from *Rxfp1*$^{-/-}$ mice was restricted to arterial cells only, whereas (b) cellular haptotaxis or migration through the layer of collagen was increased on both arterial and venous cells isolated from *Rxfp1*$^{-/-}$ mice. (c) Proliferation rate did not differ between *Rxfp1*$^{-/-}$ and WT mice. Cells were cultured for 14 days. Migration, haptotaxis and proliferation were measured over 16h time period. (*) P<0.05; (**) P<0.005; n=4.

Elastin metabolism in AVF lesions of RXFP1 deficient mice

Having observed higher elastin content in the venous outflow tract of AVF in *Rxfp1*$^{-/-}$ mice, we next assessed elastase activity in sections obtained from the venous outflow tract of the AVF. We employed the EnzChek assay, which measures fluorescence of the substrate (bovine elastin) digested by elastase. Elastase activity in AVFs from *Rxfp1*$^{-/-}$ mice was significantly reduced as compared to AVFs derived from WT mice (P=0.0001) (Figure 6).

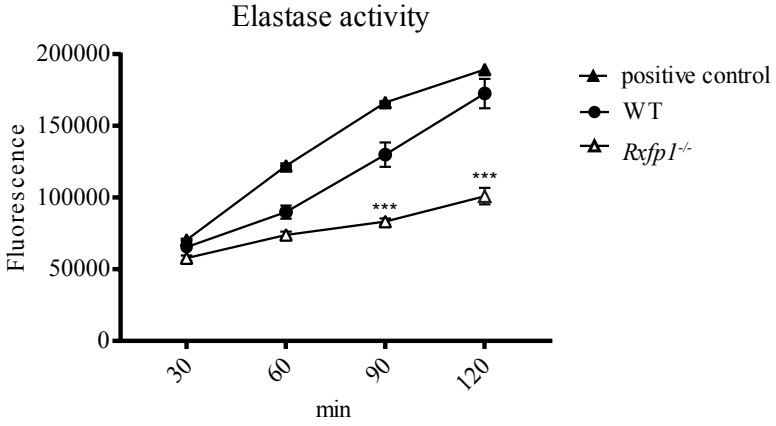

Figure 6. Kinetics of the elastase activity in the lesions of *Rxfp1*$^{-/-}$ and WT mice 14 days after surgery.
AVF tissue lysates from WT and *Rxfp1*$^{-/-}$ mice were incubated with DQ elastin at final concentrations of 25 µg/mL for the indicated time periods. Elastase activity in AVFs from *Rxfp1*$^{-/-}$ mice (empty triangles) was significantly reduced after 90 and 120 min incubation time as compared to AVFs derived from WT mice (full circles). Fluorescence was measured in a fluorescence multi-well plate reader set for excitation at 485 ± 10 nm and emission detection at 530 ± 15 nm. Porcine pancreatic elastase 0.2 U/mL was used as positive control (full triangles). Background fluorescence, determined for a no-enzyme control reaction, has been subtracted from each value. (***) P=0.0002; n=10 per group.

Ex vivo, elastin synthesis in cultured arterial and venous VSMCs isolated from *Rxfp1*$^{-/-}$ or WT mice did not differ, as mRNA expression levels of tropoelastin were similar between the groups (Supplemental Figure 5).

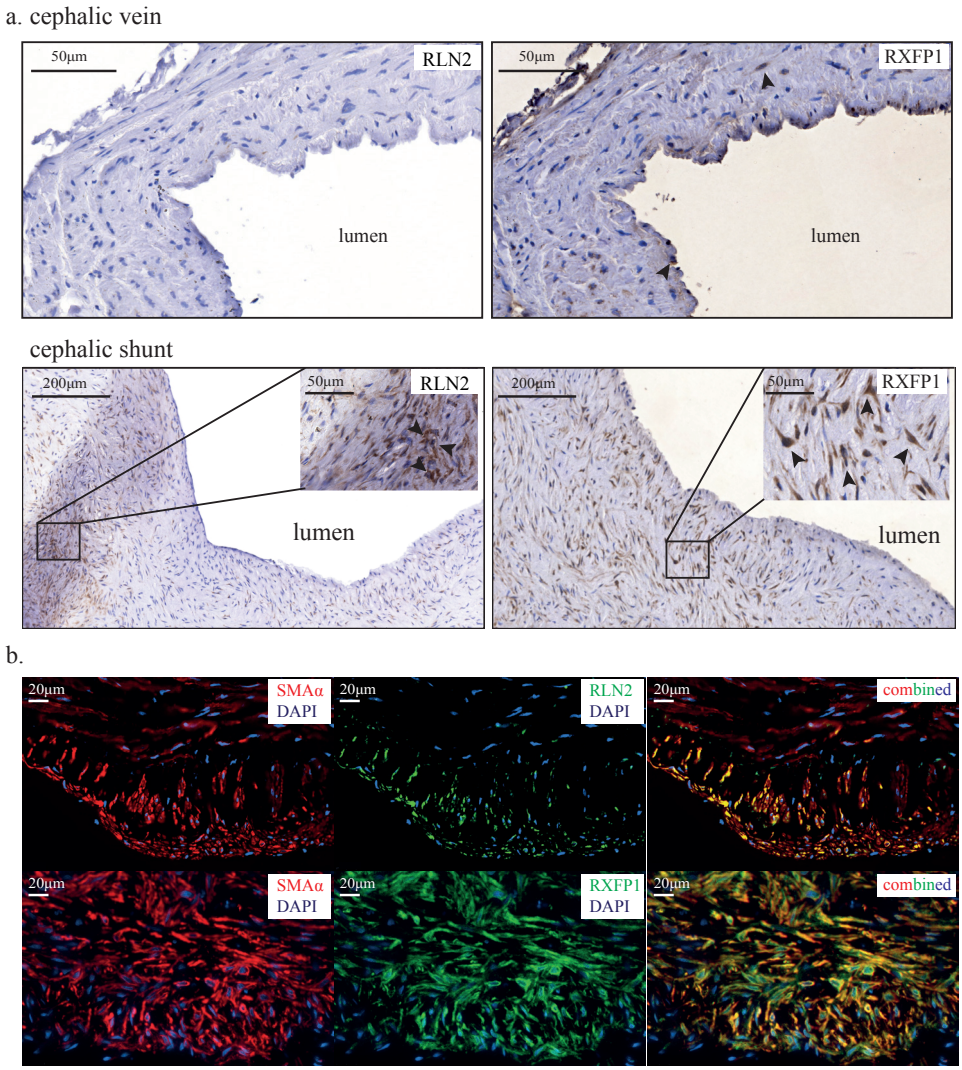

Figure 7. Expression of RLN2 and RXFP1 proteins by αSMA⁺ cells in dialysis patients.
(a) Representative images of RLN2 and RXFP1 proteins (black arrows) in human cephalic veins prior to AVF surgery and cephalic venous outflow tract from AVF. (b) Cells positive for RLN2 and RXFP1 (green color) were mainly located in the intimal region and were co-expressing SM-α-actin (αSMA, red color); n=3.

In humans RXFP1 expression increases during AVF maturation

To explore the relevance of our observations for dialysis patients, we examined three specimens of cephalic vein before AVF surgery and during surgical revisions of AVF. Immunohistochemical analysis revealed increased RLN2 and RXFP1 expression in the cephalic outflow tract of AVF, when compared to segments of cephalic veins from patients with end-stage renal failure during primary AVF surgery (Figure 7a). Cells that expressed RLN2 and RXFP1 were enriched in the intimal region of the outflow tract, and were found to co-express SM-α-actin (Figure 7b). These results strongly suggest that RLN2 and RXFP1 expression is elevated in the venous outflow tract of human AVFs, which underscores the relevance of these proteins in the process of AVF maturation in humans.

Discussion

Here, we show that RXFP1 deficiency substantially impairs outward remodeling in a murine model of AVF, while no effect on intimal hyperplasia is observed. Our findings pinpoint an increase in elastin content in the venous outflow tract in RXFP1 deficient mice linked with attenuated elastase activity as potentially being responsible for this phenotype. As such, impaired elastin degradation, in combination with enhanced vascular inflammation upon AVF surgery, likely triggers adverse vascular response in humans following the placement of an AVF.

Impaired elastin degradation and vascular remodeling in RXFP1 deficient mice

Expansion of the venous lumen and an initial vasodilatory response are prerequisites for successful AVF maturation and patency. Particularly, the process of outward remodeling plays a pivotal role in this process. While past research focused mainly on the development of strategies that aimed to reduce intimal hyperplasia, current view on AVF maturation underscores the link between impaired outward remodeling and AVF failure[42,43]. To promote outward remodeling, matrix metalloproteinases (MMPs) expression must be augmented to degrade and restructure the vascular matrix[44], of which elastic fibers are a major component. Interestingly, peri-adventitial application of recombinant elastase has been shown to stimulate outward remodeling in a rabbit-model of AVF[45]. Interestingly, this concept of pharmacological elastin degradation to promote AVF maturation is now being evaluated in phase III clinical trials[46].

Enhanced expression of relaxin is critical for ECM remodeling in the cervix and myometrium during pregnancy[47,48]. Administration of recombinant relaxin increases the activity of elastase in human myometrial cells[26]. Our discovery that RXFP1 deficiency significantly reduced elastase activity, resulting in elastic fiber accumulation in AVF lesions suggests that RXFP1 is an important regulator of elastin degradation during AVF maturation. Furthermore, it supports the concept that venous outward remodeling requires relaxin axis-mediated augmentation of elastase activity.

RXFP1 deficiency enhances vascular inflammation upon AVF surgery

Successful AVF maturation is severely hampered by excessive inflammation post-surgery. Numerous animal studies have shown that drivers of inflammatory responses, such as heme oxygenase-1 and -2 (HO-1 and HO-2) and MCP1, are linked to AVF failure[49-51]. Within the AVF, MCP1 has been found to enhance monocyte recruitment and macrophage differentiation, activate endothelial cells and stimulate VSMC proliferation[51]. In one of our previous studies, local administration of liposomal prednisolone resulted in a reduction of the inflammatory response that resulted in a sharp increase in venous outward remodeling in a murine-model of AVF[4]. Interestingly, relaxin-relaxin receptor interactions are known to mitigate vascular inflammation, by inhibiting the upregulation of pro-inflammatory cytokines[27]. In keeping with these findings, we here found that RXFP1 deficiency augments vascular inflammation in AVFs, as illustrated by a significant increase in macrophage and neutrophil numbers, as well as accumulation of MCP1 in the venous outflow tract.

Phenotypic switch of VSMCs from RXFP1$^{-/-}$ in vitro does not influence intimal hyperplasia *in vivo*.

Despite elevated levels of MCP1 in AVF lesions of *Rxfp1*$^{-/-}$ mice we unexpectedly did not observe effects on venous intimal hyperplasia. To unravel this observation, *in vitro* studies on VSMCs were performed as they play a key role in intimal hyperplasia formation and AVF maturation. We observed that RXFP1 ablation caused a phenotypic switch of both arterial and venous VSMCs from a contractile towards a synthetic phenotype. The switch from the contractile phenotype to the synthetic, is associated with increased migratory and proliferative capacity. Indeed, functional studies revealed an increase in migration of arterial cells from *Rxfp1*$^{-/-}$ mice while migration of venous cells was not altered. Surprisingly, when cells had to migrate through a layer of collagen, both arterial and venous VSMCs isolated form *Rxfp1*$^{-/-}$ mice displayed elevated migration. Collectively, these findings suggest that the surrounding and ECM architecture will ultimately determine VSMCs behavior and could potentially differ between arterial and venous VSMCs. The question arises why RXFP1 deficiency *in vivo* resulted in decreased outward remodeling and had no effect on intimal hyperplasia, whereas *in vitro* functional studies clearly show impact of RXFP1 deficiency on VSMCs migration. In this respect, it is important to notice that the efficacy of cell migration *in vivo* strongly depends on the balance between cell deformability and ECM density, of which the latter is governed by the capacity of proteolytic enzymes to degrade matrix components[52]. Interestingly, RXFP1 deficiency resulted in a significant increase in elastin content as a result of decreased elastase activity. This preserved elastin density most likely explains why the increased migratory capacity of RXFP1 deficient VSMCs *in vitro*, did not translate into enhanced intima hyperplasia in the venous outflow tract of AVF in *Rxfp1*$^{-/-}$ mice.

Alongside the well-established role for the relaxin-axis in pregnancy, the evolutionally conserved expression of RXFP1 within blood vessels of several mammals in a gender-independent fashion underscores the importance of this protein-receptor interaction in the vasculature. Our data indicate that the RLN2 and RXFP1 proteins are highly expressed in human AVF lesions, strongly suggesting that therapeutic targeting of this

pathway in the context of AVF maturation could be beneficial. In this respect, it is encouraging that clinical trials with serelaxin, a recombinant form of relaxin, have displayed promising effects in the treatment of heart failure[53]. In parallel, small-molecule agonists of RXFP1 are currently being developed[54].

Despite these advances, some aspects of our study require further discussion. Our studies were performed in healthy mice, and given that response in animals does not necessarily mimic human pathology, it is critical to remain cautious in extrapolating results derived from murine studies to patients with chronic renal failure. Another limitation of our experimental setup is the inability to perform flow measurements and cannulations of the murine AVF, as an adequate blood flow volume and the cannulability of the AVF are the main characteristics of functional hemodialysis access. Nevertheless, the present study demonstrates the functional significance of the RXFP1 pathway in AVF remodeling, implying that the RLN2-RXFP1 pathway could be a novel therapeutic target to promote maturation and longevity of AVFs for hemodialysis.

Acknowledgements

This study was supported by a grant from Leiden University Medical Center. We would like to thank Reshma A. Lalai for her excellent assistance in performing experiments and data analysis.

References

1. Schinstock, C.A., *et al.* Outcomes of arteriovenous fistula creation after the Fistula First Initiative. *Clinical journal of the American Society of Nephrology : CJASN* **6**, 1996-2002 (2011).
2. Al-Jaishi, A.A., *et al.* Patency rates of the arteriovenous fistula for hemodialysis: a systematic review and meta-analysis. *American journal of kidney diseases : the official journal of the National Kidney Foundation* **63**, 464-478 (2014).
3. Rothuizen, T.C., *et al.* Arteriovenous access failure: more than just intimal hyperplasia? *Nephrology, dialysis, transplantation : official publication of the European Dialysis and Transplant Association - European Renal Association* **28**, 1085-1092 (2013).
4. Wong, C., *et al.* Liposomal prednisolone inhibits vascular inflammation and enhances venous outward remodeling in a murine arteriovenous fistula model. *Scientific reports* **6**, 30439 (2016).
5. Wong, C.Y., *et al.* Vascular remodeling and intimal hyperplasia in a novel murine model of arteriovenous fistula failure. *Journal of vascular surgery* (2013).
6. Bezhaeva, T., *et al.* Deficiency of TLR4 homologue RP105 aggravates outward remodeling in a murine model of arteriovenous fistula failure. *Scientific reports* **7**, 10269 (2017).
7. Krishnamoorthy, M.K., *et al.* Hemodynamic wall shear stress profiles influence the magnitude and pattern of stenosis in a pig AV fistula. *Kidney international* **74**, 1410-1419 (2008).
8. Liang, M., *et al.* Migration of smooth muscle cells from the arterial anastomosis of arteriovenous fistulas requires Notch activation to form neointima. *Kidney international* **88**, 490-502 (2015).
9. Roy-Chaudhury, P., *et al.* Cellular phenotypes in human stenotic lesions from haemodialysis vascular access. *Nephrology, dialysis, transplantation : official publication of the European Dialysis and Transplant Association - European Renal Association* **24**, 2786-2791 (2009).
10. Roy-Chaudhury, P., *et al.* Pathogenetic role for early focal macrophage infiltration in a pig model of arteriovenous fistula (AVF) stenosis. *The journal of vascular access* **15**, 25-28 (2014).
11. Zhao, J., *et al.* Dual Function for Mature Vascular Smooth Muscle Cells During Arteriovenous Fistula Remodeling. *Journal of the American Heart Association* **6**(2017).
12. Conrad, K.P., Debrah, D.O., Novak, J., Danielson, L.A. & Shroff, S.G. Relaxin modifies systemic arterial resistance and compliance in conscious, nonpregnant rats. *Endocrinology* **145**, 3289-3296 (2004).
13. Feng, S., Bogatcheva, N.V., Kamat, A.A., Truong, A. & Agoulnik, A.I. Endocrine effects of relaxin overexpression in mice. *Endocrinology* **147**, 407-414 (2006).
14. Cernaro, V., *et al.* Relaxin: new pathophysiological aspects and pharmacological perspectives for an old protein. *Medicinal research reviews* **34**, 77-105 (2014).
15. Jeyabalan, A., Shroff, S.G., Novak, J. & Conrad, K.P. The vascular actions of relaxin. *Advances in experimental medicine and biology* **612**, 65-87 (2007).
16. Sherwood, O.D. Relaxin's physiological roles and other diverse actions. *Endocrine reviews* **25**, 205-234 (2004).
17. Debrah, D.O., Conrad, K.P., Jeyabalan, A., Danielson, L.A. & Shroff, S.G. Relaxin increases cardiac output and reduces systemic arterial load in hypertensive rats. *Hypertension (Dallas, Tex. : 1979)* **46**, 745-750 (2005).
18. Conrad, K.P. & Shroff, S.G. Effects of relaxin on arterial dilation, remodeling, and mechanical properties. *Current hypertension reports* **13**, 409-420 (2011).
19. Debrah, D.O., *et al.* Relaxin regulates vascular wall remodeling and passive mechanical properties in mice. *Journal of applied physiology (Bethesda, Md. : 1985)* **111**, 260-271 (2011).

20. Chan, S.L. & Cipolla, M.J. Relaxin causes selective outward remodeling of brain parenchymal arterioles via activation of peroxisome proliferator-activated receptor-gamma. *FASEB journal : official publication of the Federation of American Societies for Experimental Biology* **25**, 3229-3239 (2011).
21. Samuel, C.S., Lekgabe, E.D. & Mookerjee, I. The effects of relaxin on extracellular matrix remodeling in health and fibrotic disease. *Advances in experimental medicine and biology* **612**, 88-103 (2007).
22. Samuel, C.S. & Hewitson, T.D. Relaxin and the progression of kidney disease. *Current opinion in nephrology and hypertension* **18**, 9-14 (2009).
23. Chow, B.S., *et al.* Relaxin requires the angiotensin II type 2 receptor to abrogate renal interstitial fibrosis. *Kidney international* (2014).
24. Zhou, X., *et al.* Relaxin inhibits cardiac fibrosis and endothelial-mesenchymal transition via the Notch pathway. *Drug design, development and therapy* **9**, 4599-4611 (2015).
25. Bennett, R.G., Heimann, D.G., Singh, S., Simpson, R.L. & Tuma, D.J. Relaxin decreases the severity of established hepatic fibrosis in mice. *Liver international : official journal of the International Association for the Study of the Liver* **34**, 416-426 (2014).
26. Chen, B., Wen, Y., Yu, X.Y. & Polan, M.L. Relaxin increases elastase activity and protease inhibitors in smooth muscle cells from the myometrium compared with cells from leiomyomas. *Fertility and sterility* **91**, 1351-1354 (2009).
27. Brecht, A., Bartsch, C., Baumann, G., Stangl, K. & Dschietzig, T. Relaxin inhibits early steps in vascular inflammation. *Regulatory peptides* **166**, 76-82 (2011).
28. Novak, J., *et al.* Evidence for local relaxin ligand-receptor expression and function in arteries. *FASEB journal : official publication of the Federation of American Societies for Experimental Biology* **20**, 2352-2362 (2006).
29. Jelinic, M., *et al.* Localization of relaxin receptors in arteries and veins, and region-specific increases in compliance and bradykinin-mediated relaxation after in vivo serelaxin treatment. *FASEB journal : official publication of the Federation of American Societies for Experimental Biology* **28**, 275-287 (2014).
30. Bathgate, R.A., *et al.* Relaxin family peptides and their receptors. *Physiological reviews* **93**, 405-480 (2013).
31. Horton, J.S., Yamamoto, S.Y. & Bryant-Greenwood, G.D. Relaxin modulates proinflammatory cytokine secretion from human decidual macrophages. *Biology of reproduction* **85**, 788-797 (2011).
32. Leo, C.H., *et al.* Vascular actions of relaxin: nitric oxide and beyond. *British journal of pharmacology* **174**, 1002-1014 (2017).
33. Kamat, A.A., *et al.* Genetic targeting of relaxin and insulin-like factor 3 receptors in mice. *Endocrinology* **145**, 4712-4720 (2004).
34. Wong, C.Y., *et al.* A Novel Murine Model of Arteriovenous Fistula Failure: The Surgical Procedure in Detail. *Journal of visualized experiments : JoVE*, e53294 (2016).
35. Shin, D., *et al.* Expression of ephrinB2 identifies a stable genetic difference between arterial and venous vascular smooth muscle as well as endothelial cells, and marks subsets of microvessels at sites of adult neovascularization. *Developmental biology* **230**, 139-150 (2001).
36. Owens, G.K., Kumar, M.S. & Wamhoff, B.R. Molecular regulation of vascular smooth muscle cell differentiation in development and disease. *Physiological reviews* **84**, 767-801 (2004).
37. Lacolley, P., Regnault, V., Nicoletti, A., Li, Z. & Michel, J.B. The vascular smooth muscle cell in arterial pathology: a cell that can take on multiple roles. *Cardiovascular research* **95**, 194-204 (2012).

38. Ichii, T.*, et al.* Fibrillar collagen specifically regulates human vascular smooth muscle cell genes involved in cellular responses and the pericellular matrix environment. *Circulation research* **88**, 460-467 (2001).
39. Thyberg, J. & Hultgardh-Nilsson, A. Fibronectin and the basement membrane components laminin and collagen type IV influence the phenotypic properties of subcultured rat aortic smooth muscle cells differently. *Cell and tissue research* **276**, 263-271 (1994).
40. Hocevar, B.A. & Howe, P.H. Analysis of TGF-beta-mediated synthesis of extracellular matrix components. *Methods in molecular biology* **142**, 55-65 (2000).
41. Kingsley, K.*, et al.* ERK1/2 mediates PDGF-BB stimulated vascular smooth muscle cell proliferation and migration on laminin-5. *Biochemical and biophysical research communications* **293**, 1000-1006 (2002).
42. Lee, T. & Misra, S. New Insights into Dialysis Vascular Access: Molecular Targets in Arteriovenous Fistula and Arteriovenous Graft Failure and Their Potential to Improve Vascular Access Outcomes. *Clinical journal of the American Society of Nephrology : CJASN* **11**, 1504-1512 (2016).
43. Guzman, R.J., Abe, K. & Zarins, C.K. Flow-induced arterial enlargement is inhibited by suppression of nitric oxide synthase activity in vivo. *Surgery* **122**, 273-279; discussion 279-280 (1997).
44. Chan, C.Y., Chen, Y.S., Ma, M.C. & Chen, C.F. Remodeling of experimental arteriovenous fistula with increased matrix metalloproteinase expression in rats. *Journal of vascular surgery* **45**, 804-811 (2007).
45. Burke SK, F.F., LaRochelle A, Mendenhall HV Local application of recombinant human type I pancreatic elastase (PRT-201) to an arteriovenous fistula (AVF) increases AVF blood flow in a rabbit model. . *J Am Soc Nephrol* **19: 252–253A** (2008)**.**
46. Peden, E.K.*, et al.* Arteriovenous fistula patency in the 3 years following vonapanitase and placebo treatment. *Journal of vascular surgery* **65**, 1113-1120 (2017).
47. Finlay, G.A., O'Donnell, M.D., O'Connor, C.M., Hayes, J.P. & FitzGerald, M.X. Elastin and collagen remodeling in emphysema. A scanning electron microscopy study. *The American journal of pathology* **149**, 1405-1415 (1996).
48. Chen, B., Wen, Y., Yu, X. & Polan, M.L. Elastin metabolism in pelvic tissues: is it modulated by reproductive hormones? *American journal of obstetrics and gynecology* **192**, 1605-1613 (2005).
49. Kang, L.*, et al.* A new model of an arteriovenous fistula in chronic kidney disease in the mouse: beneficial effects of upregulated heme oxygenase-1. *American journal of physiology. Renal physiology* **310**, F466-476 (2016).
50. Kang, L.*, et al.* Functioning of an arteriovenous fistula requires heme oxygenase-2. *American journal of physiology. Renal physiology* **305**, F545-552 (2013).
51. Juncos, J.P.*, et al.* MCP-1 contributes to arteriovenous fistula failure. *Journal of the American Society of Nephrology : JASN* **22**, 43-48 (2011).
52. Wolf, K.*, et al.* Physical limits of cell migration: control by ECM space and nuclear deformation and tuning by proteolysis and traction force. *The Journal of cell biology* **201**, 1069-1084 (2013).
53. Teerlink, J.R.*, et al.* Serelaxin, recombinant human relaxin-2, for treatment of acute heart failure (RELAX-AHF): a randomised, placebo-controlled trial. *Lancet* **381**, 29-39 (2013).
54. Xiao, J.*, et al.* Identification and optimization of small-molecule agonists of the human relaxin hormone receptor RXFP1. *Nat Commun* **4**(2013).

Supplementary material

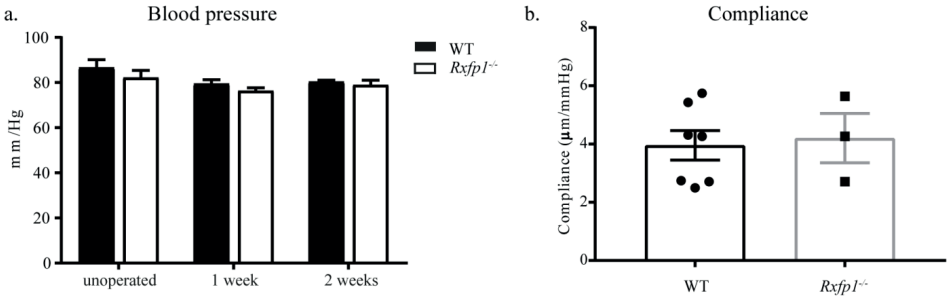

Supplementary Figure 1. (a) Arterial blood pressure levels did not differ between *Rxfp1*$^{-/-}$ and WT mice over the course of AVF maturation. n=5 per group. (b) Basal arterial compliance was also similar between *Rxfp1*$^{-/-}$ and WT mice. n=7 WT; n=3 *Rxfp1*$^{-/-}$.

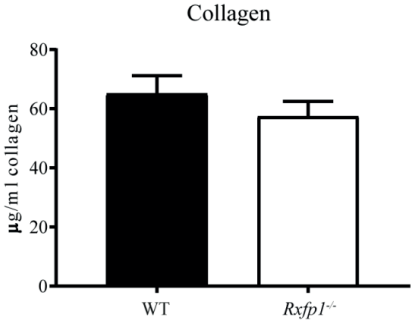

Supplementary Figure 2. Effect of RXFP1 deficiency on collagen content *in vivo*.
Collagen was analyzed in venous AVF sections from *Rxfp1*$^{-/-}$ and WT mice. Total collagen content did not differ between the groups. n = 10 per group.

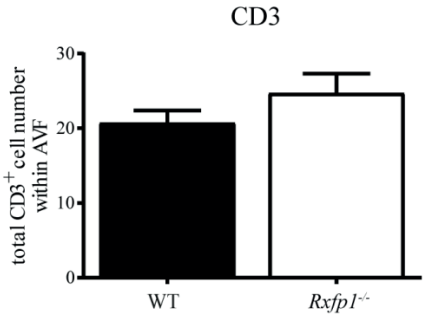

Supplementary Figure 3. Quantification of CD3⁺ T-cells in the AVF lesions 14 days after surgery. n=10 per group.

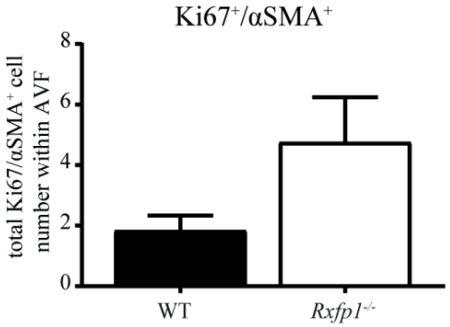

Supplementary Figure 4. Effect of RXFP1 deficiency on VSMCs proliferation *in vivo*.
Quantification of Ki67⁺/αSMA⁺ cells in AVF lesions of *Rxfp1*$^{-/-}$ and WT mice 14 days after AVF surgery. n=11 per group.

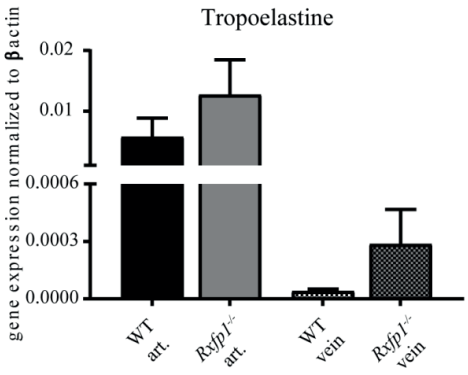

Supplementary Figure 5. Tropoelastine mRNA expression levels in cultured primary arterial and venous cells isolated from Rxfp1-/- and WT mice. n=4 per group.

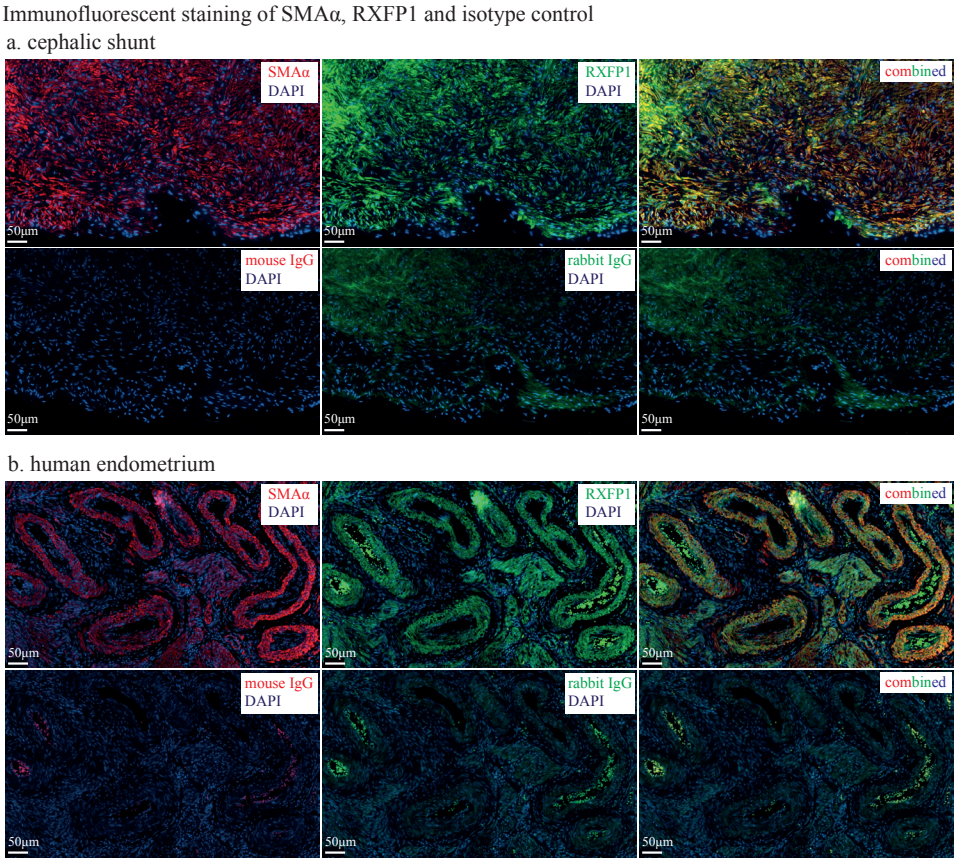

Supplementary Figure 6. Immunofluorescence RXFP1 antibody validation.
For immunofluorescent staining of double positive SMA$^+$, RXFP1$^+$ cells in (a) cephalic shunt and (b) endometrium after primary antibody sections were counterstained with Alexa 568 conjugated goat anti mouse IgG2a (1:250; Molecular probes A21134) for SMAα and Alexa 488 conjugated secondary goat anti rabbit IgG (1:250; Molecular probes A11008) for RXFP1. Mouse or rabbit IgG were used as negative controls. Nuclei were visualized with ProLong™ Gold Antifade Mountant with DAPI.

Table 1. Primers used for in vitro experiments

Gene	Forward primer	Reversed primer
ephrinB2	ACGGTCCAACAAGACGTCCA	GCTGTTGCCATCGGTGCTA
MyHC	TGGCTAGCAGCTTGTCAGGAA	GCCTTGCGTACTCTATCACTCATG
calponin	GAAGGCAGGAACATCATTGGA	CCTGCTGACTGGCAAACTTG
caldesmon	GCCGTTCAAGTGCTTCACTC	TGTCAATCTTGGAGACTACTGCT
Col1	TGACTGGAAGAGCGGAGAGT	GTTCGGGCTGATGTACCAGT
Fibronectin	ATGTGGACCCCTCCTGATAGT	GCCCAGTGATTTCAGCAAAGG
TGFβ	GCAACATGTGGAACTCTACCAGAA	GACGTCAAAAGACAGCCACTCA
PDGF	CAAGAAGCGGCCATGAATCAG	CGGCCCTAGTGAGTTGTTGT
tropoelastin	GGTTGTTCAGACTACAATCTGACC	CAACTTTGCCCAAATGACTCTCC
βactin	AGGTCATCACTATTGGCAACGA	CCAAGAAGGAAGGCTGGAAAA